P5A-ATPases control the ER translocation of Wnt for neuronal migration

Tingting Li[1,2,3], Xiaoyan Yang[1,2,3], Zhigang Feng[1], Wang Nie[1,2,3], Yan Zou[1,2,4,*]

[1]School of Life Science and Technology, ShanghaiTech University, Shanghai, 201210, China

[2]Institute of Neuroscience, State Key Laboratory of Neuroscience, CAS Center for Excellence in Brain Science and Intelligence Technology, Shanghai Institutes for Biological Sciences, Chinese Academy of Sciences, Shanghai, 200031, China

[3]University of Chinese Academy of Sciences, Beijing 100049, China

[4]Lead Contact

[*]Correspondence: zouyan@shanghaitech.edu.cn

Key words: P5A-ATPase, Wnt signaling, neuronal migration, *C. elegans*.

Abstract

Wnt family are conserved secreted proteins required for developmental patterning and tissue homeostasis. Research into the mechanisms that influence intracellular maturation and intercelluar signal transduction of Wnt proteins has proved fruitful. However, the knowledge of how Wnt enters into the endoplasmic reticulum (ER) for processing and secretion is still limited. Here we report that CATP-8/P5A-ATPase directs neuronal migration in *C. elegans* by controlling EGL-20/Wnt biogenesis. Our genetic and biochemical analyses demonstrate that CATP-8 control the ER targeting of EGL-20/Wnt through the hydrophobic core region in EGL-20 signal sequence. We further show that regulation of Wnt biogenesis by P5A-ATPase is conserved in human cells. These findings reveal physiological roles of P5A-ATPase in neuronal development and identify Wnt proteins as direct substrates of P5A-ATPase to be translocated into the ER.

Introduction

Wnt proteins comprise an evolutionarily conserved morphogen family which plays a fundamental role in development patterning and tissue homeostasis. Wnt proteins are secreted from producing cells, triggering a variety responses including cell fate specification, polarity and migration in target cells. Dysregulations of Wnt signaling are associated with a variety of developmental deficits and diseases (Clevers, 2006).

Wnt family are glycoproteins, forming a globular secondary structure through intramolecular disulfide bonds among 24 highly conserved cysteines. Functional Wnt requires multi-layers of posttranslational modifications, such as acylation, glycosylation and sulfation, which are critical for correct folding and subsequent secretion (Willert and Nusse, 2012). The journey of Wnt processing, folding and trafficking starts in the ER. However, upon translation, how Wnt targets to the ER is largely unknown.

Secreted Wnt proteins influence neural connectivity by patterning neuronal migration, axon guidance, and synapse formation. The Q neuroblasts in *C. elegans* offer an ideal model to study neuronal migration and Wnt signaling (Chai et al., 2018). The bilateral Q neuroblast on the left side (QL) and Q neuroblast on the right side (QR) are born between V4 and V5 seam cells in the posterior worm, on the left and right sides symmetrically (Sulston and Horvitz, 1977). Although QL and QR undergo similar cell division processes, they migrate towards opposite directions. QL migrates posteriorly, differentiating into PQR, PVM and SDQL neurons (Figure 1A and 1B). In contrast, QR migrates anteriorly, producing AQR, AVM and SDQR neurons. The migration of Q neuroblasts is activated by EGL-20/Wnt proteins secreted from the posterior (Coudreuse et al., 2006). Wnt secretion requires endocytosis of Wnt-transport factor MIG-14/Wls by Retromer complex, as well as proper folding by protein disulfide isomerase PDI-1 (Coudreuse et al., 2006; Pan et al., 2008; Torpe et al., 2019; Yang et al., 2008). Binding of EGL-20/Wnt to Frizzled receptors LIN-17 and MIG-1 in the QL cell leads to activation of the canonical Wnt signaling with BAR-1/β-catenin stabilization and nuclear localization (Harris et al., 1996; Maloof et al., 1999; Sawa et al., 1996), which induces the transcription of target genes including

mab-5 (Harris et al., 1996; Salser and Kenyon, 1992; Whangbo and Kenyon, 1999). The transduced signal initiates cytoskeleton rearrangement through WAVE/WASP coordination and hippo kinase (Feng et al., 2017; Zhu et al., 2016). In addition, Q cell polarity is regulated by UNC-40/DCC, PTP-3 and MIG-21 to determine its exposure to EGL-20/Wnt (Honigberg and Kenyon, 2000; Sundararajan and Lundquist, 2012).

P-type ATPases comprise a conserved transporter superfamily and can be divided into five subfamilies: P1- through P5-ATPases. Typical P-type ATPases pump ions (P1- through P3-ATPases) or lipids (P4-ATPases) across cellular membranes with the energy of ATP hydrolysis (Palmgren and Nissen, 2011), while substrates of P5-ATPases had been undefined and speculated to be cations or lipids for a long time (Sorensen et al., 2015; Sorensen et al., 2019; Suzuki and Shimma, 1999). P5 subfamily consists of two subgroups: P5A-ATPase and P5B-ATPase. Recently, several studies provide insights into the substrates and gating mechanisms of P5-ATPases. Veen et al. demonstrated that ATP13A2, a human P5B-ATPase ortholog, transports lysosomal polyamine into the cytosol (van Veen et al., 2020). Next, we demonstrated that CATP-8/P5A-ATPase regulates dendrite branching by controlling the ER translocation of DMA-1 receptor in *C. elegans* (Feng et al., 2020). Another two papers reported that P5A-ATPases safeguard ER integrity by removing mislocalized mitochondria tail-anchored (TA) proteins from the ER (McKenna et al., 2020; Qin et al., 2020). These findings suggest that P5-ATPases diverse from other P-type subfamilies and have much larger substrates like polyamines for P5B or polypeptides for P5A.

Expression of P5A-ATPase is abundant in mouse brain with the highest expression coinciding with the peak of neurogenesis (Weingarten et al., 2012). Moreover, human genetic analysis revealed that mutation in P5A-ATPase is associated with intellectual disability, attention deficit hyperactivity disorder (ADHD) and a host of developmental malformations and defects (Anazi et al., 2017). Despite the implication of P5A-ATPase in neural development, most sudies on P5A-ATPase are carried out in yeast or cell culture. Only our previous work and Qin et al. have reported that dendrite branching in *C. elegans* requires P5A-ATPase to control the

biogenesis of DMA-1 guidance receptor (Feng et al., 2020; Qin et al., 2020). However, DMA-1 is not very conservative to its ortholog in mammals. Therefore, physiological functions of P5A-ATPase in metazoans, particularly in nervous system, remain to be elucidated.

Here, we report that CATP-8/P5A-ATPase patterns neuronal migration in *C. elegans*. Our genetic and biochemical analyses reveal that that CATP-8 acts in Wnt-producing cells to control the ER translocation of EGL-20/Wnt. Interestingly, the hydrophobicity of core region in signal sequences determine the translocation dependency on P5A-ATPase. We further demonstrate that P5A-ATPase directly controls Wnt biogenesis in human cells in a conserved manner. Collectively, we identify Wnt as a substrate of P5A-ATPase to be translocated into the ER for secretion to direct neuronal migration.

Results

CATP-8/P5A-ATPase Is Required for Neuronal Migration

To understand the physiological roles of P5A-ATPase in nervous system, we carried out a phenotypic investigation of *catp-8* mutants using multiple neuron-type specific reporters, and observed severe migration defects of PQR neuron. PQR neurons in wild-type (WT) animals are next to the anus in the tail (Figure 1B). However, in the two *catp-8* null alleles (Figure 1D), *catp-8(yan22*) and *catp-8(yan32)*, a majority of PQR neurons locate near the anterior deirid in the head (Figure 1C and 1E). Transgenic expression of *catp-8* driven by endogenous promoter fully rescued PQR migration defects in *catp-8* mutants (Figure 1F), suggesting *catp-8* is required for PQR posterior localization.

As stated above, PQR are differentiated from QL neuroblast, accompanied by two other QL descendent cells, PVM and SDQL (Figure 1A). To explore whether migration of the whole QL lineage is affected by *catp-8* mutation, we also examined PVM and SDQL neurons. Similar as PQR neurons, both PVM and SDQL neurons migrate more anteriorly in *catp-8* mutants than in WT worms (Figure S1). We thus hypothesized that *catp-8* mutation impairs early direction of the whole QL lineage. To

test this idea, we perform time-lapse imaging on the developing Q neuroblasts in live animals. As shown in Figure 1G, the first division descendants of QL neuroblast, QL.a and QL.p cells, already made an opposite migration decision toward the anterior in *catp-8* mutants, whereas their counterparts in WT animals protrude toward the posterior. Taken together, our results suggest that *catp-8* is required to direct QL posterior migration.

***catp-8* Acts in the Canonical Wnt Pathway to control QL migration**

The asymmetric migration of QL and QR neuroblasts are determined by whether the transcription of the Hox gene *mab-5* is intrinsically activated. The *mab-5*-expressing QL descendants migrate posteriorly, whereas lack of *mab-5* expression in the QR progeny results in anteriorly directed migration (Salser and Kenyon, 1992). In *mab-5* loss-of-function (lf) mutants, both QL and QR descendants migrate toward the anterior. On the contrary, in *mab-5* gain-of-function (gf) mutant, which ectopically expresses *mab-5* in both QL and QR lineages, all their progeny cells migrate toward the posterior (Salser and Kenyon, 1992). To uncover the genetic program underlying *catp-8* involved neuronal migration, we first tested the epistatic interaction between *mab-5* and *catp-8*. We found that *mab-5(lf);catp-8(yan22)* double mutants display similar QL migration defects to *mab-5(lf)* single mutants, while *mab-5(gf)* completely suppresses QL migration defects caused by *catp-8(yan22)* (Figure 2B), suggesting that *catp-8* acts upstream of *mab-5*. Then we assessed whether *mab-5* is properly expressed in *catp-8* mutants using a *Pmab-5::GFP* reporter. Interestingly, *mab-5* expression is lost in anteriorly-localized PQR cells in *catp-8* mutants, while posteriorly-localized PQR cells in *catp-8* mutants still retain *mab-5* expression (Figure 2C). Therefore, defective PQR migration in *catp-8* mutants is likely due to *mab-5* activation failure.

The *mab-5*-dependent QL migration is activated by a canonical Wnt pathway (Harris et al., 1996). Wnt ligand EGL-20 is perceived by Frizzled receptors LIN-17 and MIG-1 in the QL cell, then transduced by MIG-5/Dishevelled to release BAR-1/β-catenin from inhibition by PRY-1/Axin. Stabilized β-catenin is thus

translocated to the nucleus where it initiates the expression of many genes including *mab-5* (Figure 2A). To investigate whether *catp-8* acts through the canonical Wnt pathway to control QL migration, we tested the genetic interactions between *catp-8* and those key factors. We found that *catp-8* mutation enhanced QL migration defect in Frizzled receptor mutant *lin-17* or *mig-1*, while had no effect on the defects in *mig-5*/Dishevelled and *bar-1*/β-catenin mutation (Figure 2D). Notably, mutation of *pry-1*/Axin, the negative-acting factor in this pathway, suppressed defective anterior displacement of QL in *catp-8* mutants (Figure 2D). Taken together, we concluded that *catp-8* acts upstream of *pry-1* in the canonical Wnt pathway for QL migration.

To determine the role of *catp-8* in the canonical Wnt pathway, we further explored the genetic interactions between *catp-8* and known factors involved in EGL-20/Wnt biogenesis. As shown in Figure 2E, *catp-8* enhanced QL defective migration in anterior positions in *mig-14*/Wls and *vps-29*/Retromer but not in *egl-20*/Wnt mutants, further supporting that *catp-8* and *egl-20* act in the same pathway. Moreover, epistatic analysis suggests that *catp-8* functions upstream of *egl-20* since overexpression of *egl-20* fully rescued QL migration defects in *catp-8* (Figure 2E).

catp-8 Acts Cell-Non-Autonomously from Wnt-Producing Cells to Control Neuronal Migration

On the basis of our genetic results, we proposed that *catp-8* likely acts cell-non-autonomously in the Wnt-producing cells to control QL migration. Hence, we investigated the expression pattern of *catp-8* using an N-terminal *gfp* knock-in strain *catp-8(yan27 ki[gfp::catp-8])*. However, we found *catp-8* expressed ubiquitously in both PQR neuron and its surrounding hypodermis from which EGL-20/Wnt is secreted (Figure 3A). To determine cell-autonomous requirement of *catp-8*, we then used *egl-20* promoter or *egl-17* promoter to drive *catp-8* expression specifically in Wnt-producing cells or in QL descendants. To our surprise, *catp-8* overexpression driven by either *egl-20* or *egl-17* promoter was able to rescue the QL migration defects in *catp-8* mutants (Figure 3B). Then we tried *spon-1* promoter (Josephson et al., 2016), which is also expressed in Wnt-producing cells and gives

similar result as *egl-20* promoter (Figure 3B). However, when we examined the expression pattern of *egl-17* promoter carefully, we found that it has a weak but broader expression in PQR neighboring cells (Figure 3A). Therefore, rescue of *catp-8* driven by *egl-17* promoter may be attributed to the expression outside of PQR and is not conclusive. To obtain exclusive expression of *catp-8* in QL descendants, we designed a binary expression system combining *Pegl-17::Cre* and *Ptoe-2::loxp::stop::loxp::gfp::catp-8* (Figure 3C). The overlap of *toe-2* (Gurling et al., 2014) promoter and *egl-17* promoter provides a more restricted expression of *catp-8* in QL descendants (Figure 3D), which could not rescue the QL migration defects caused by *catp-8* (Figure 3E). Altogether, our results suggest a cell-non-autonomous role of *catp-8* in QL migration.

catp-8 controls ER translocation of EGL-20/Wnt through EGL-20 Signal Sequence

Since *catp-8* acts upstream of *egl-20*/Wnt in the EGL-20 producing cells, we next asked whether *catp-8* regulates *egl-20*/Wnt. Using an integrated *Pegl-20::egl-20::GFP* reporter, we found that *catp-8* depletion significantly reduced EGL-20::GFP level, while re-expression of *catp-8* restored EGL-20::GFP intensity (Figure 4A). Western blot of confirmed reduction of EGL-20::GFP in *catp-8* mutants (Figure 4D). In contrast, mRNA levels of *egl-20* measured by real-time RT-PCR were similar in both WT and *catp-8* (Figure 4E). Therefore, we conclude that *catp-8* regulates EGL-20 at protein level.

Previous study showed that CATP-8 is required for the ER translocation of DMA-1 receptor for dendrite branching in a signal sequence dependent manner (Feng et al., 2020). Since upon translation, Wnt proteins translocate into the ER to be intracellular processed and sorted for secretion (Willert and Nusse, 2012), we wondered whether CATP-8 controls the ER translocation of EGL-20/Wnt through EGL-20 signal sequence (EGL-20SS). To test this, we constructed an engineered protein EGL-20SS::GFP::3*GLY::FLAG. If this engineered protein is able to translocate into the ER, the three glycosylation sites (3*Gly) would become

glycosylated and thus generate a larger protein than its calculated molecular weight. As expected, this EGL-20SS guided protein entered into the ER in WT but failed in *catp-8* mutants (Figure 4B), suggesting that its translocation is dependent on CATP-8. To confirm the requirement of EGL-20SS for CATP-8 regulated EGL-20 biogenesis, we utilized CRISPR-Cas9 to replace the endogenous EGL-20SS with a previously described CATP-8 independent signal sequence, PAT-3SS (Feng et al., 2020). Indeed, PAT-3SS knock-in at *egl-20* locus rescued QL migration in *catp-8* mutants (Figure 4C and 4F). Collectively, our data demonstrated that CATP-8 controls EGL-20/Wnt biogenesis through the recognition of specific signal sequence.

Signal sequences generally comprise characteristic tripartite architecture: a positive-charged N-terminal region, a hydrophobic core region and a C-terminal cleavage site by signal peptidases (Owji et al., 2018). Since both EGL-20SS and PAT-3SS only contain no-charged residues (Figure 4G), we wonder whether hydrophobicity is the key factor for CATP-8-dependent translocation. Hence, we mutated EGL-20SS and PAT-3SS by increasing their hydrophobicity in the core region (Figure 4G), and then assessed their translocation efficiency in *ATP13A1*/P5A-ATPase knock out (KO) HEK293FT cells. We found that EGL-20SS(M) displayed higher dependence on ATP13A1 than EGL-20SS. Intriguingly, increased hydrophobicity turned PAT-3SS(M) to rely on ATP13A1 completely (Figure 4H). Taken together, these results suggest that P5A-ATPase likely recognizes certain signal sequences by the high hydrophobicity in the core region.

P5A ATPases Directly Control Wnt Biogenesis in a Conserved Manner

Since both P5A ATPase and Wnt proteins are present in higher organisms, we next asked whether the regulation of EGL-20/Wnt biogenesis by CATP-8 in *C. elegans* is evolutionarily conserved in mammals. To test this, we transfected human WNT1 in both WT and *ATP13A1* KO cells and found WNT1 protein level are dramatically reduced in *ATP13A1* KO cells (Figure 5A). Moreover, similar to the observation in *C. elegans*, Wnt1 signal sequence (Wnt1SS) is essential for the *ATP13A1*-dependent WNT1 biogenesis (Figure 5B). These results reveal the functional conservation of

P5A-ATPases in regulating ER translocation of Wnt proteins.

We next sought to determine whether Wnt1 is a direct substrate to be translocated by ATP13A1. As translocation is a very transient process, it is difficult to capture the interactions by co-immunoprecipitation. We thus employed PUP-IT proximal labeling system (Liu et al., 2018) to detect whether there are physical interactions between ATP13A1 and WNT1. We transfected ATP13A1 fused with the proximity ligase PafA as a bait and either WNT1SS or PAT-3SS as a prey. If Wnt1SS is the substrate of ATP13A1, we expected that PafA-ATP13A1 catalyzes the ligation of a small protein Biotin-PupE to Wnt1SS guided protein. Indeed, WNT1SS but not PAT-3SS guided protein was labeled with Biotin-PupE by PafA-ATP13A1 (Figure 5C), suggesting a direct and specific control of WNT1 translocation by ATP13A1.

Discussion

In this study, we identified CATP-8/P5A-ATPase as a key factor to direct neuronal migrations through regulating EGL-20/Wnt biogenesis. Our genetic and biochemical analyses demonstrate that CATP-8/P5A-ATPase controls the ER translocation of EGL-20/Wnt by specifically recognizing the hydrophobic core region in signal sequences. Moreover, the effect of P5A-ATPase on Wnt biogenesis is recapitulated in human cells, implying a conserved role of P5A-ATPase on Wnt-mediated developmental events.

Although numerous studies have been focused on Wnt trafficking and signal transduction, it is still not clear how Wnt enters into the ER for subsequent processing and secretion. Wnt family harbor hydrophobic signal sequences at the N-terminus, which are hallmarks for secreted proteins. Therefore, the signal sequence guided ER translocation of Wnt was speculated to be similar to other secreted proteins. However, our results demonstrate that P5A-ATPase is specifically required for the ER translocation of certain transmembrane (TM) proteins like DMA-1 (Feng et al., 2020) and secreted proteins like Wnt. P5A-ATPase emerges in the eukaryotes and gains distinct capacity for larger substrates like polypeptides (Feng et al., 2020; McKenna et al., 2020; Qin et al., 2020). Interestingly, putative substrates of P5A-ATPase in

metazoans, Wnt and DMA-1, are important for cell-cell communications and have large biosynthesis demands in relatively short developmental critical windows, which might be an extra burden for their producing cells. For example, EGL-20/Wnt is secreted from several cells in the worm tail and forms a gradient to pattern multiple early developmental events. DMA-1 is synthesized by two tiny PVD neurons and trafficked onto huge dendritic arborizations covering the whole worm body to perceive guidance cues from hypodermis (Dong et al., 2013; Liu and Shen, 2011). An interesting view is that P5A-ATPase may function as a freeway to the ER for high demanding proteins to be efficiently translocated, or to prevent the jam by heavy protein load to the essential translocon Sec61.

Intriguingly, different substrates of P5A-ATPase are likely transported in opposite directions. First, our studies demonstrate that P5A-ATPase directly controls the translocation from the cytosol to the ER of certain proteins with highly hydrophobic N-terminal signal sequences. Second, McKenna and Qin et al. show that P5A-ATPase functions as a dislocase to remove mistargeted mitochondria TA proteins from the ER to the cytosol (McKenna et al., 2020; Qin et al., 2020). McKenna et al. speculated that proteins with N-terminal signal sequences are generally less hydrophobic and often have positive-charged N-termini than TM, which might lead to their ER insertion in a wrong topology. They proposed that P5A-ATPase might also remove these wrong topological proteins from the ER, providing addition opportunities for correct ER targeting (McKenna et al., 2020). However, estimated from our data in Figure 4B, the vast majority of EGL-20 translocation is dependent on CATP-8. In this sense, CATP-8 has to remove wrong targeting EGL-20 repeatedly, which is inefficient and at high cost. Therefore, the mechanistic basis how P5A-ATPase recognizes different substrates and thus transports them in the opposite directions requires further study. The substrate specificity of P5A-ATPase might come from high hydrophobicity of signal sequences, as enhancement of hydrophobicity increases their translocation dependence on P5A-ATPase.

Directed neuronal migration is critical for the development of functional nervous system. We identified Wnt proteins as direct substrates of P5A-ATPases in neuronal

patterning, which may explain the observation that ATP13A1 mutation in human is associated with neurodevelopmental disorders (Anazi et al., 2017). Considering ubiquitous expressions and pleiotropic phenotypes of P5A-ATPase (Anazi et al., 2017; Feng et al., 2020; Qin et al., 2020; Sorensen et al., 2015; Weingarten et al., 2012), there are more clients of P5A-ATPase in other cellular contexts yet to be identified for better understanding of the physiological roles of P5A-ATPase in metazoans.

ACKNOWLEDGEMENTS

We thank Drs. Zhiyong Shao and Yingchuan Qi for reagents. We thank Drs. Yingchuan Qi, Huanhu Zhu, and Xiajing Tong for helpful discussions. We thank the Molecular Imaging Core Facility (MICF) at ShanghaiTech University for assistance on confocal microscopy. Some strains were provided by the CGC, which is funded by NIH Office of Research Infrastructure Programs (P40 OD010440). This study was supported by the National Natural Science Foundation of China (No.31571047) and the Start-up grant from ShanghaiTech University.

AUTHOR CONTRIBUTIONS

Conceptualization, T.L., Z.F. and Y.Z.; Investigation, T.L., Z.F., X.Y., W.N. and Y.Z.; Writing – Original Draft, Y.Z. and T.L.; Writing – Review & Editing, Y.Z.; Funding Acquisition, Y.Z.; Supervision, Y.Z.

DECLARATION OF INTERESTS

The authors declare no competing interests.

REFERENCES

Anazi, S., Maddirevula, S., Salpietro, V., Asi, Y.T., Alsahli, S., Alhashem, A., Shamseldin, H.E., AlZahrani, F., Patel, N., Ibrahim, N., *et al.* (2017). Expanding the genetic heterogeneity of intellectual disability. Hum Genet *136*, 1419-1429.

Brenner, S. (1974). The genetics of Caenorhabditis elegans. Genetics *77*, 71-94.

Chai, Y., Zhu, Z., and Ou, G. (2018). Migration of Q Cells in Caenorhabditis elegans. Methods Mol Biol *1749*, 239-255.

Clevers, H. (2006). Wnt/beta-catenin signaling in development and disease. Cell *127*, 469-480.

Coudreuse, D.Y.M., Roel, G., Betist, M.C., Destree, O., and Korswagen, H.C. (2006). Wnt gradient formation requires retromer function in Wnt-producing cells. Science *312*, 921-924.

Dickinson, D.J., Ward, J.D., Reiner, D.J., and Goldstein, B. (2013). Engineering the Caenorhabditis elegans genome using Cas9-triggered homologous recombination. Nat Methods *10*, 1028-1034.

Dong, X., Liu, O.W., Howell, A.S., and Shen, K. (2013). An extracellular adhesion molecule complex patterns dendritic branching and morphogenesis. Cell *155*, 296-307.

Eisenmann, D.M. (2005). Wnt signaling. WormBook.

Feng, G., Zhu, Z., Li, W.J., Lin, Q., Chai, Y., Dong, M.Q., and Ou, G. (2017). Hippo kinases maintain polarity during directional cell migration in Caenorhabditis elegans. EMBO J *36*, 334-345.

Feng, Z.G., Zhao, Y.P., Li, T.T., Nie, W., Yang, X.Y., Wang, X.J., Wu, J.G., Liao, J., and Zou, Y. (2020). CATP-8/P5A ATPase Regulates ER Processing of the DMA-1 Receptor for Dendritic Branching. Cell Rep *32*.

Gurling, M., Talavera, K., and Garriga, G. (2014). The DEP domain-containing protein TOE-2 promotes apoptosis in the Q lineage of C. elegans through two distinct mechanisms. Development *141*, 2724-2734.

Harris, J., Honigberg, L., Robinson, N., and Kenyon, C. (1996). Neuronal cell migration in C. elegans: regulation of Hox gene expression and cell position. Development *122*, 3117-3131.

Honigberg, L., and Kenyon, C. (2000). Establishment of left/right asymmetry in neuroblast migration by UNC-40/DCC, UNC-73/Trio and DPY-19 proteins in C.elegans. Development *127*, 4655-4668.

Josephson, M.P., Miltner, A.M., and Lundquist, E.A. (2016). Nonautonomous Roles of MAB-5/Hox and the Secreted Basement Membrane Molecule SPON-1/F-Spondin in Caenorhabditis elegans Neuronal Migration. Genetics *203*, 1747-1762.

Judith Buentzel, S.T. (2017). The Use of Glycosylation Tags as Reporters for Protein Entry into the Endoplasmic Reticulum in Yeast and Mammalian Cells. In: Schrader M. (eds) Peroxisomes., Vol 1595 (Humana Press, New York, NY).

Liu, O.W., and Shen, K. (2011). The transmembrane LRR protein DMA-1 promotes dendrite branching and growth in C. elegans. Nat Neurosci *15*, 57-63.

Liu, Q., Zheng, J., Sun, W.P., Huo, Y.B., Zhang, L.Y., Hao, P.L., Wang, H.P., and Zhuang, M. (2018). A proximity-tagging system to identify membrane protein-protein interactions. Nat Methods *15*, 715-+.

Maloof, J.N., Whangbo, J., Harris, J.M., Jongeward, G.D., and Kenyon, C. (1999). A Wnt signaling pathway controls Hox gene expression and neuroblast migration in C-elegans. Development *126*, 37-49.

McKenna, M.J., Sim, S.I., Ordureau, A., Wei, L., Harper, J.W., Shao, S., and Park, E. (2020). The endoplasmic reticulum P5A-ATPase is a transmembrane helix dislocase. Science *369*.

Mello, C., and Fire, A. (1995). DNA transformation. Method Cell Biol *48*, 451-482.

Owji, H., Nezafat, N., Negahdaripour, M., Hajiebrahimi, A., and Ghasemi, Y. (2018). A comprehensive review of signal peptides: Structure, roles, and applications. Eur J Cell Biol *97*, 422-441.

Palmgren, M.G., and Nissen, P. (2011). P-Type ATPases. Annu Rev Biophys *40*, 243-266.

Pan, C.L., Baum, P.D., Gu, M., Jorgensen, E.M., Clark, S.G., and Garriga, G. (2008). C. elegans AP-2 and retromer control Wnt signaling by regulating mig-14/Wntless. Dev Cell *14*, 132-139.

Qin, Q., Zhao, T., Zou, W., Shen, K., and Wang, X. (2020). An Endoplasmic Reticulum ATPase Safeguards Endoplasmic Reticulum Identity by Removing Ectopically Localized Mitochondrial Proteins. Cell Rep *33*, 108363.

Salser, S.J., and Kenyon, C. (1992). Activation of a C-Elegans Antennapedia Homolog in Migrating

Cells Controls Their Direction of Migration. Nature *355*, 255-258.

Sawa, H., Lobel, L., and Horvitz, H.R. (1996). The Caenorhabditis elegans gene lin-17, which is required for certain asymmetric cell divisions, encodes a putative protein similar to seven-transmembrane protein similar to the Drosophila Frizzle protein. Gene Dev *10*, 2189-2197.

Sorensen, D.M., Holen, H.W., Holemans, T., Vangheluwe, P., and Palmgren, M.G. (2015). Towards defining the substrate of orphan P5A-ATPases. Bba-Gen Subjects *1850*, 524-535.

Sorensen, D.M., Holen, H.W., Pedersen, J.T., Martens, H.J., Silvestro, D., Stanchev, L.D., Costa, S.R., Pomorski, T.G., Lopez-Marques, R.L., and Palmgren, M. (2019). The P5A ATPase Spf1p is stimulated by phosphatidylinositol 4-phosphate and influences cellular sterol homeostasis. Molecular Biology of the Cell *30*, 1069-1084.

Sulston, J.E., and Horvitz, H.R. (1977). Post-embryonic cell lineages of the nematode, Caenorhabditis elegans. Dev Biol *56*, 110-156.

Sundararajan, L., and Lundquist, E.A. (2012). Transmembrane Proteins UNC-40/DCC, PTP-3/LAR, and MIG-21 Control Anterior-Posterior Neuroblast Migration with Left-Right Functional Asymmetry in Caenorhabditis elegans. Genetics *192*, 1373-+.

Suzuki, C., and Shimma, Y. (1999). P-type ATPase spf1 mutants show a novel resistance mechanism for the killer toxin SMKT. Mol Microbiol *32*, 813-823.

Torpe, N., Gopal, S., Baltaci, O., Rella, L., Handley, A., Korswagen, H.C., and Pocock, R. (2019). A Protein Disulfide Isomerase Controls Neuronal Migration through Regulation of Wnt Secretion. Cell Rep *26*, 3183-+.

van Veen, S., Martin, S., Van den Haute, C., Benoy, V., Lyons, J., Vanhoutte, R., Kahler, J.P., Decuypere, J.P., Gelders, G., Lambie, E., *et al.* (2020). ATP13A2 deficiency disrupts lysosomal polyamine export. Nature *578*, 419-424.

Wang, X., Li, T., Hu, J., Feng, Z., Zhong, R., Nie, W., Yang, X., and Zou, Y. (2021). In vivo imaging of a PVD neuron in Caenorhabditis elegans. STAR Protoc *2*, 100309.

Weingarten, L.S., Dave, H., Li, H., and Crawford, D.A. (2012). Developmental expression of P5 ATPase mRNA in the mouse. Cell Mol Biol Lett *17*, 153-170.

Whangbo, J., and Kenyon, C. (1999). A Wnt signaling system that specifies two patterns of cell migration in C-elegans. Mol Cell *4*, 851-858.

Willert, K., and Nusse, R. (2012). Wnt Proteins. Csh Perspect Biol *4*.

Yang, P.T., Lorenowicz, M.J., Silhankova, M., Coudreuse, D.Y.M., Betist, M.C., and Korswagen, H.C. (2008). Wnt signaling requires retromer-dependent recycling of MIG-14/Wntless in Wnt-producing cells. Dev Cell *14*, 140-147.

Zhu, Z., Chai, Y., Jiang, Y., Li, W., Hu, H., Li, W., Wu, J.W., Wang, Z.X., Huang, S., and Ou, G. (2016). Functional Coordination of WAVE and WASP in C. elegans Neuroblast Migration. Dev Cell *39*, 224-238.

FIGURE LEGEND

Figure 1. *catp-8* Is Required for Neuronal Migration

(A) Schematic depicting QL neuroblast lineage. QL neuroblast undergoes three rounds of asymmetric divisions to yield two apoptotic cells (yellow circles with X) and three neurons PQR, PVM, SDQL.

(B) Diagram showing cell divisions and migration of QL neuroblast. V1 through V6 depict the positions of six seam cells. Color code is the same as in (A).

(C) Representative images of PQR positions in WT, *catp-8(yan22)*, *catp-8(yan32)*, and *catp-8(yan22)* with a single copy transgene of *yanTi9 [Pcatp-8::catp-8]*. PQR neurons were visualized by a fluorescent marker *lqIs58[gcy-32::cfp]*. Scale bar, 100 μm.

(D) Schematic of *catp-8* gene showing molecular lesions of *catp-8(yan22)* and *catp-8(yan32)* mutants. Arrowhead indicates the position of the point mutation in the *yan22* allele.

(E) Quantifications of POR positions in (C). Data are presented as mean ± SEM. N numbers are shown in the brackets. ****, $P<0.0001$ (One-sided ANOVA with the Tukey correction).

(F) Time-lapse imaging of QL descendant migrations at indicated time points after the first round of cell division. QL descendants were visualized by a fluorescent marker *rdvIs1[Pegl-17::Myr-mCherry; Pegl-17::mig-10::YFP; Pegl-17::mCherry-TEV-S::his-24]*. The dashed lines indicate worm positions with arrowheads pointing to A (Anterior) and P (Posterior) respectively. Scale bar, 10 μm.

Figure 2. *catp-8* Acts in the Wnt/β-catenin Pathway to Control PQR Migration.

(A) Schematic diagram of the canonic Wnt/β-catenin pathway required for QL migration, modified from (Eisenmann, 2005).

(B) Quantifications of PQR positions in indicated genotypes, showing that *catp-8* acts upstream of *mab-5*. Data are presented as mean ± SEM. N numbers are shown in the brackets. ****, $P<0.0001$; ns, not significant (One-sided ANOVA with the Tukey correction).

(C) Representative images of *mab-5* expression shown by a *Pmab-5::gfp* transgene in WT and *catp-8* mutants. Diagram showing PQR positions in indicated genotypes. PQR neurons were visualized using a *Pegl-17::mcherry* fluorescence marker. Arrowheads point to PQR. Scale bar, 10 μm.

(E-F) Quantifications of PQR positions in indicated genotypes, showing that *catp-8*

449 acts in the canonical Wnt pathway. Data are presented as mean ± SEM. N numbers are
450 shown in the brackets. **, *P*<0.01; ***, *P*<0.001; ****, *P*<0.0001; ns, not significant
451 (One-sided ANOVA with the Tukey correction).
452
453 **Figure 3. *catp-8* Functions Cell-Non-Autonomously in the Wnt Producing Cells**
454 **to Direct PQR Migration.**
455 (A) Representative images showing CATP-8 expression in both Wnt producing cells
456 and Q neuroblast. Green: CATP-8 expression shown by a GFP knocked in the *catp-8*
457 genomic locus. Red: expression pattern of *egl-20* promoter shown by
458 *Pegl-20::NLS-mCherry* (top), expression of *egl-17* promoter in PQR and the midline
459 shown by *rdvIs1* (middle), expression of *egl-17* promoter in QL shown by *rdvIs1*
460 (bottom).
461 (B) Quantifications of PQR positions in indicated genotypes. Data are presented as
462 mean ± SEM. N numbers are shown in the brackets. ****, *P*<0.0001 (One-sided
463 ANOVA with the Tukey correction).
464 (C) Diagram depicting the constructs of the Cre-dependent binary expression system
465 used in (D). *Pgene2* refers to either *egl-17* promoter or *egl-20* promoter.
466 (D) Representative images of *catp-8* expressions (Green) by the Cre-dependent binary
467 expression system. PQR neurons were visualized by a *Pgcy-32::mcherry* transgene.
468 Scale bar, 10 μm.
469 (E) Quantifications of defective PQR migration in indicated genotypes, showing that
470 overexpressing *catp-8* in Wnt-producing cells but not in PQR rescues PQR migration
471 defects in *catp-8* mutants. Data are presented as mean ± SEM. N numbers are shown
472 in the brackets. ***, *P*<0.001; ns, not significant (One-sided ANOVA with the Tukey
473 correction).
474
475 **Figure 4. *catp-8* Controls ER translocation of EGL-20/Wnt.**
476 (A) Representative images of *egl-20::GFP* expression in WT, *catp-8(yan22)*, and
477 *catp-8(yan22)* with a single copy transgene of *yanTi9 [Pcatp-8::catp-8]*. Scale bar, 20
478 μm.

(B) Western blot of EGL-20SS-GFP-3*GLY-FLAG in WT and *catp-8(yan22)*. Bars indicate quantifications of the glycosylated proteins. Data are presented as mean ± SEM. ****, $P<0.0001$ (Tukey's multiple comparisons test).

(C) Representative images of PQR positions in WT, *catp-8(yan22)*, and *catp-8(yan22)* with a PAT-3SS knock-in to replace the endogenous EGL-20SS. PQR neurons were visualized by a fluorescent marker *lqIs58[gcy-32::cfp]*. Scale bar, 100 μm.

(D) Western blot showing EGL-20::GFP protein levels in (A). Bars indicate quantifications of EGL-20::GFP and are presented as mean ± SEM. *, $P<0.05$ (Tukey's multiple comparisons test).

(E) Real-time RT-PCR showing mRNA abundance of *egl-20* in WT and *catp-8(yan22)* mutants. Data are presented as mean ± SEM. n.s., not significant (Student's *t* test).

(F) Quantifications of PQR positions in (E). Data are presented as mean ± SEM. N numbers are shown in the brackets. ****, $P<0.0001$ (One-sided ANOVA with the Tukey correction).

(G) Signal sequences of EGL-20, PAT-33, and their mutants with higher hydrophobicity. The hydrophobicity was calculated by the ΔG prediction server v1.0 (https://dgpred.cbr.su.se/index.php?p=TMpred).

(H) Western blot showing translocation efficiency of signal sequences in (G), assessed by the glycosylated band over Actin. DHFR is to generate a protein at suitable size. Opsin tag is a glycosylation reporter for protein entry into the ER (Judith Buentzel, 2017). Data are presented as mean ± SEM. **, $P<0.01$; ns, not significant (Tukey's multiple comparisons test).

Figure 5. P5A-ATPases function conservatively to regulate Wnt biogenesis.

(A) Western blot of transfected WNT1 in control, *ATP13A1* KO, and *ATP13A1* KO cells with *ATP13A1* overexpression. Data are presented as mean ± SEM. *, $P<0.05$; ***, $P<0.001$ (Tukey's multiple comparisons test).

(B) Western blot of transfected WNT1SS-FLAG-DHFR-Opsin in control, *ATP13A1* KO, and *ATP13A1* KO cells with *ATP13A1* overexpression. Data are presented as mean ± SEM. *, $P<0.05$; ns, not significant (Tukey's multiple comparisons test).

(C) Western blot showing proximal labeling of WNT1SS-FLAG-DHFR-Opsin by PafA-ATP13A1. Asterisk indicates Biotin-PupE labeled WNT1SS-FLAG-DHFR-Opsin.

Figure S1. *catp-8* Is Required for PVM and SDQL Migration, Related to Figure 1.

(A) Representative images of PVM positions in WT and *catp-8(yan22)*. PVM neurons were labeled by a fluorescent marker *zdIs5[Pmec-4::gfp]*. Scale bar, 50 μm.

(B) Quantifications of PVM positions in (A). Data are presented as mean ± SEM. N numbers are shown in the brackets. ****, $P<0.0001$ (One-sided ANOVA with the Tukey correction).

(C) Representative images of SDQL positions in WT and *catp-8(yan22)*. SDQL neurons were labeled by a fluorescent marker *Ex[Pgcy-35::mcherry]*. Scale bar, 50 μm.

(D) Quantifications of SDQL positions in (C). Data are presented as mean ± SEM. N numbers were shown in the brackets. ****, $P<0.0001$ (One-sided ANOVA with the Tukey correction).

527 **KEY RESOURCES TABLE**

REAGENT or RESOURCE	SOURCE	IDENTIFIER
Antibodies		
Mouse anti-FLAG	Sigma	Cat# F1804; RRID:AB_262044
Mouse anti-GFP	Abmart	Cat# M20004; RRID:AB_2619674
Rabbit anti-ATP13A1	Proteintech	Cat# 16244-1-AP; RRID:AB_10015282
Donker anti-Rabbit	Jackson Immunoresearch	Cat# 711-035-152; RRID:AB_10015282
Rabbit anti-Mouse	Sigma	Cat# A9044; RRID:AB_258431
Rabbit anti-b-Actin	Marine Biological Laboratory	Cat# PM053-7; RRID:AB_10697035
Bacterial and Virus Strains		
OP50	CGC	https://www.cgc.edu/strain/OP50
Chemicals, Peptides, and Recombinant Proteins		
KOD-Plus-Neo	TOYOBO	Cat# KOD-401
KOD One™ PCR Master Mix	TOYOBO	Cat# KMM-101
Experimental Models: Cell Lines		
HEK293FT	ATCC	RRID:CVCL_6911
Experimental Models: Organisms/Strains		
C. elegans strain, see Table S1	This paper	N/A
Oligonucleotides		
see Table S2	This paper	N/A
Recombinant DNA		
Plasmid: *pDD122*	Addgene	RRID:Addgene_47550
Plasmid: *pDD162*	Addgene	RRID:Addgene_47549
Plasmid: *Pgcy-32::mcherry*	This paper	N/A
Plasmid: *Pgcy-35::mcherry*	This paper	N/A
Plasmid: *Pcatp-8::catp-8*	This paper	N/A
Plasmid: *Pegl-17::catp-8*	This paper	N/A
Plasmid: *Pspon-1::catp-8]*	This paper	N/A
Plasmid: *Pegl-20::catp-8*	This paper	N/A
Plasmid: *Pegl-20::nls::mcherry*	This paper	N/A
Plasmid: *Ptoe-2::loxp::stop::loxp::gfp::catp-8*	This paper	N/A
Plasmid: *Pegl-20::nls::CRE*	This paper	N/A
Plasmid: *Pegl-17::nls::CRE*	This paper	N/A

Plasmid: *Pegl-20::egl-20*	This paper	N/A
Plasmid: *Prpl-28::egl-20SS::gfp::Gly::FLAG*	This paper	N/A
Plasmid: *Prpl-28::cwn-1::gfp::Gly::FLAG*	This paper	N/A
Plasmid: *pEGFP.C1-egl-20::gfp*	This paper	N/A
Plasmid: *pEGFP.C1-cwn-1::gfp*	This paper	N/A
Plasmid: *pEGFP.C1-lin-44::gfp*	This paper	N/A
Plasmid: *pEGFP.C1-cwn-2::gfp*	This paper	N/A
Plasmid: *pEGFP.C1-mom-5::gfp*	This paper	N/A
Plasmid: *pEGFP.C1-WNT1SS::FLAG::DHFR::Opsin*	This paper	N/A
Plasmid: *pEGFP.C1-WNT1::FLAG::Opsin*	This paper	N/A

EXPERIMENTAL MODEL AND SUBJECT DETAILS

Experimental Materials

C. elegans strains were cultured and maintained as described (Brenner, 1974). Details and a complete list of strains in this study are shown in Table S1. The HEK293FT cell line was obtained from ATCC (American Type Culture Collection).

METHOD

Molecular Biology and Transgenesis

We used standard molecular biology techniques for cloning and plasmid construction. Most of the plasmid constructs were generated in pSM vector backbone, more details see Key Resources Table. Germline transformation of C. elegans was performed using standard techniques (Mello and Fire, 1995). The co-injection marker plasmid and the concentration are as follows, *pCFJ104* at 5 ng/µl, *pCFJ90* at 2.5 ng/µl, *odr-1::gfp* at 60 ng/µl, or *odr-1::rfp* at 60 ng/µl.

Scoring Migration Defects of QL Neuroblast Descendants

PQR was assayed using *lqIs58[gcy-32::cfp]* in L4 animals. PVM and AVM were visualized with *zdIs5[Pmec-4::gfp]*. SDQL was assayed using extrachromosomal

arrays *Pgcy-35::mcherry*. Migration defects in QL neuroblast descendants (PQR, PVM, SDQL) depend on neuron positions in worm. We quantified the neuron position in L4 or young adult animals. We chose never ring, vulva and anus as fiduciary markers. The relative position of PQR is calculated as the distance between never ring and PQR divided by the distance between never ring and anus. The relative positions of SDQL and PVM are calculated as the distance between SDQL or PVM and vulva divided by the distance between never ring and anus, neurons posterior to vulva are calculated as positive values and neurons anterior to vulva are calculated as negative values respectively.

Imaging

Detail imaging procedures were performed as described (Wang et al., 2021) with slight modifications as follows. Animals were anesthetized with 5 mmol/L levamisole in M9 buffer, and then mounted on 2% (w/v) agarose pads. PQR neuron in L4 animal was visualized with *lqIs58[pcy-32::gfp]* and imaged using OLYMPUS BX53 fluorescent microscope with a UPlanSApo 20x/0.75 objective. The CellSens software is used to process the image. To analyze the position of other neurons, *zdIs5[Pmec-4::gfp]* marked AVM and PVM in L2 animals, extrachromosomal arrays *(Pgcy-35::mcherry)* marked SDQL in L4 animals, we used a Nikon Spinning Disk confocal microscope (TI2+CSU+W1) with Photometrics Prime 95B camera, W1 spinning disk head, the 488/561 nm excitation laser and a 60×/1.40 N.A oil immersion objective. Maximum-intensity projections were generated using ImageJ (NIH).

To image the fluorescent marker strains *rdvIs1[Pegl-17::mcherry]*, *muIs16 [mab-5::GFP]*, *ki[gfp::catp-8]*, *muIs49[egl-20::GFP]*, and transgenic arrays *Pegl-20::nls::mcherry*, we used Zeiss Axio Observer Z1 microscope (Carl Zeiss) equipped with an alpha Plan-Apochromat 63x/1.46 NA objective. ImageJ software (NIH) was used to process the images.

Time-Lapes Imaging of Neuronal Migration

C. elegans L1 larvae were anesthetized with 2.5 mmol/L levamisole in M9 buffer, and

577 then mounted on 2% (w/v) agarose pads. Slides were sealed with 2:1
578 vaseline/paraplast tissue embedding medium. Images were acquired using a Zeiss
579 Axio Observer Z1 microscope (Carl Zeiss) equipped with an alpha Plan-Apochromat
580 63x/1.46 NA objective, Yokogawa camera adapter, 561 nm laser and Hamamatsu
581 camera. QL neuroblast migration was visualized using *rdvIs1[Pegl-17::mCherry]*, a
582 stack at 1 um intervals with mCherry exposure time of 3.5 s at every 15 min. ImageJ
583 software (NIH) was used to process the images.
584
585 **CRISPR/Cas9-Mediated Genomic Editing**
586 To generate *yan125* mutant by CRISPR/Cas9 as described (Dickinson et al., 2013),
587 *Peft-3::cas9* (50 ng/µl), *U6::egl-20-sg#1* (25 ng/µl, target
588 sequence:5'-TATTTGTTCTCCTCGTTTA-3'), *U6::egl-20-sg#2* (25 ng/µl, target
589 sequence:5'-AAACTTACAGCCAGTTATA-3') and *pCFJ104* (5 ng/µl) were injected
590 into N2 strain. F1 worms were screened for successful knock-out by PCR. F2 worms
591 were cloned out without co-injection marker, genotyped by PCR, and sequenced to
592 confirm.
593 To replace EGL-20 (1-18 aa) signal sequence with PAT-3 (1-20 aa) signal
594 sequence, coding sequence of PAT-3 signal sequence was inserted in *pSM-egl-20*
595 vector via long primers. Two homologous arms were 679 bp (5'-arm) and 654 bp
596 (3'-arm) respectively. Repair template (50 ng/µl), *U6::egl-20-sg#1* (25 ng/µl),
597 *U6::egl-20-sg#2* (25 ng/µl), pCFJ104 (5 ng/µl) were injected into *catp-8(yan22)*. F1
598 worms were screened for successfully insertion using PCR, F2 worms without
599 co-injection marker were cloned out, genotyped by PCR, and verified by sequencing.
600 To rescue the PQR migration defects in *catp-8(yan22)*, a single copy insertion of
601 *yanTi9[Pcatp-8::catp-8]* was generated by CRISPR-Cas9 in *catp-8(yan22)*. The
602 promoter of *catp-8* from N2 genomic DNA and *catp-8* cDNA were amplified and
603 inserted in *ttTi5605* vector. Repair template (50 ng/µl), *pDD122* (50 ng/µl), *pCFJ104*
604 (5 ng/µl) and *pCFJ90* (2.5 ng/µl) were injected into *catp-8(yan22)*. F1 worms were
605 screened for successfully insertion using PCR. F2 worms without co-injection marker
606 were cloned out, genotyped by PCR and confirmed by sequencing.

607

608 **Western Blot**

609 We synchronized early L1 larvae by hatching them in M9 buffer, and resuming
610 feeding on regular OP50 NGM plates till they grow to L4 stage. Worms were
611 harvested and washed for three times with M9 buffer, and the pellet was lysed in
612 Laemmli sample buffer (32.9 mM Tris-HCl, pH 6.8, 13.2% glycerol, 1.05% SDS, 2.5%
613 2-mercaptoethanol and 0.005% bromophenol blue). Pellets were repeatedly boiled for
614 5 min and then vortexed for 1 min, until most of the worms were broken. The lysates
615 were spun at 13,000 rpm for 10 min at 4°C. Then supernatants were collected and
616 analyzed using western blots with mouse monoclonal anti-GFP (1:1000, Abmart),
617 Anti-β-Actin pAb-HRP-DirecT (1:5000, Medical & Biological Laboratories) and
618 HRP-conjugated Rabbit antibody to mouse (1:10,000, Sigma).

619 Plasmids were transfected into control or ATP13A1 KO cells, and then cell
620 lysates were extracted by NP40 lysis buffer (150 mM NaCl, 0.5% NP40 and 50 mM
621 Tris-HCl pH 7.4, 1mM EDTA, 10% glycerol) containing 1% Protease Inhibitor stock
622 (Bimake) for 30 min on ice. The soluble fraction of the cell lysates was isolated via
623 centrifugation at 12,000 rpm for 10 min at 4°C. Laemmli sample buffer was added to
624 the supernatant. Then the samples were heated at 65°C for 10 min, resolved via
625 SDS-PAGE gel electrophoreses, and analyzed using Western blot with the rabbit
626 polyclonal anti-ATP13A1 (1:2000, proteintech), mouse anti-FLAG (1:1000, sigma),
627 HRP-conjugated donkey anti-rabbit (1:10000, Jackson Immunoresearch), and
628 HRP-conjugated Rabbit antibody to mouse (1:30,000, Sigma).

629

630 **Real-Time RT-PCR**

631 We synchronized L1 larvae by bleaching adult animals to obtain eggs to hatch on
632 NGM plate with OP50. L1 worm was collected and lysed in 1 mL Trizol reagent
633 (Vazyme) by freeze and thaw. Total RNA extraction was followed by
634 reverse-transcription with random primers and HiScript II Q RT SuperMix for qPCR
635 (Vazyme). Relative abundance of *egl-20* and actin was quantified with real-time PCR
636 using TB Green Premix Ex TaqII (Tli RNase H Plus, Takara).

637

638 **Statistical Analysis**

639 Quantification of neuron (PQR, PVM, SDQL) positions along the anterior-posterior
640 axis of the worm body was One-way ANOVA followed by Tukey's multiple
641 comparisons test (Prism; GraphPad Software). For western blot, ImageJ Software
642 (NIH) was used to analyze the grayscale values from three biological repeats.
643 Statistical comparisons were conducted using Tukey's multiple comparisons test.
644 Statistical significance is indicated as n.s., not significant; *, $P < 0.05$; **, $P < 0.01$;
645 ***, $P < 0.001$; ****, $P < 0.0001$.

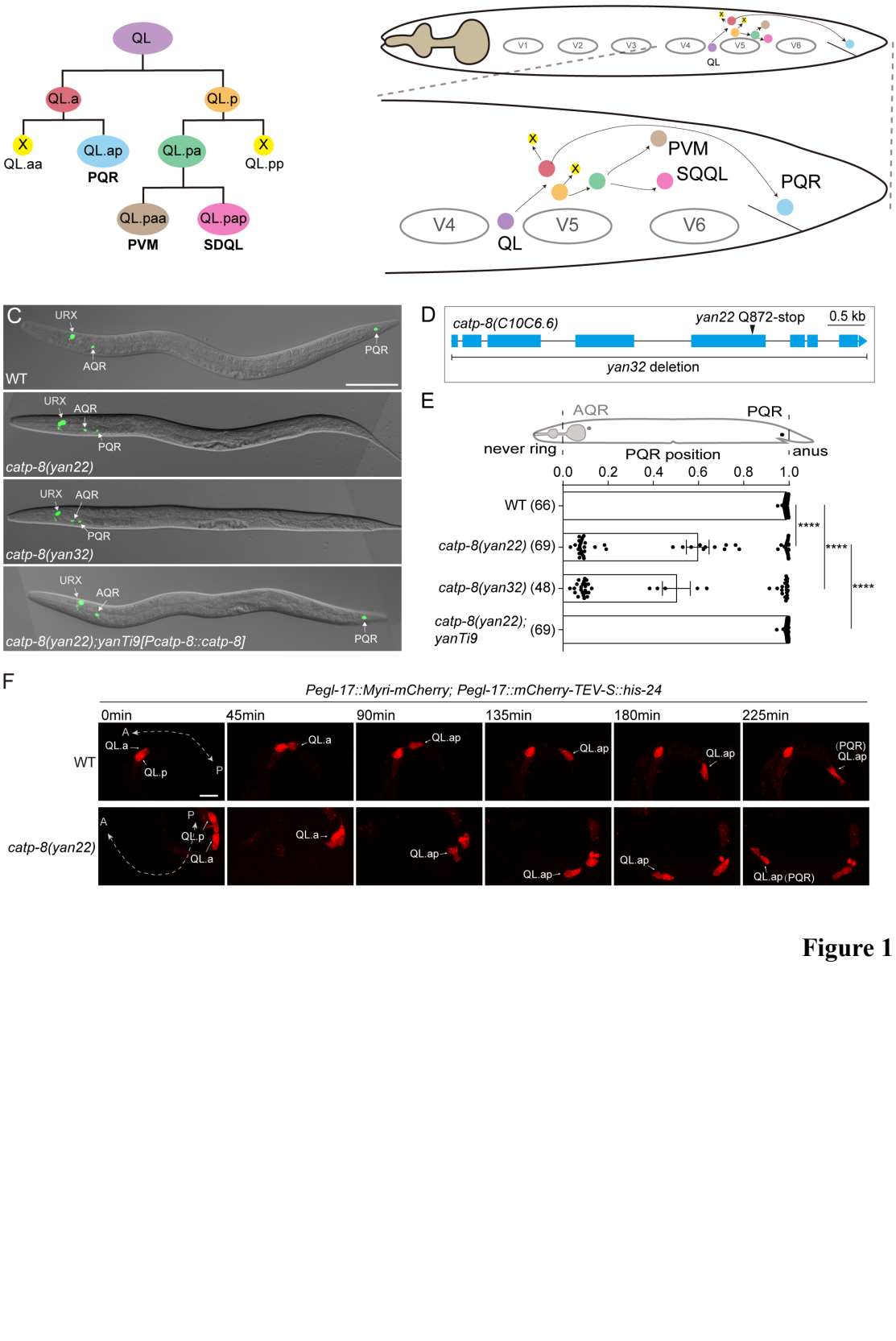

Figure 1

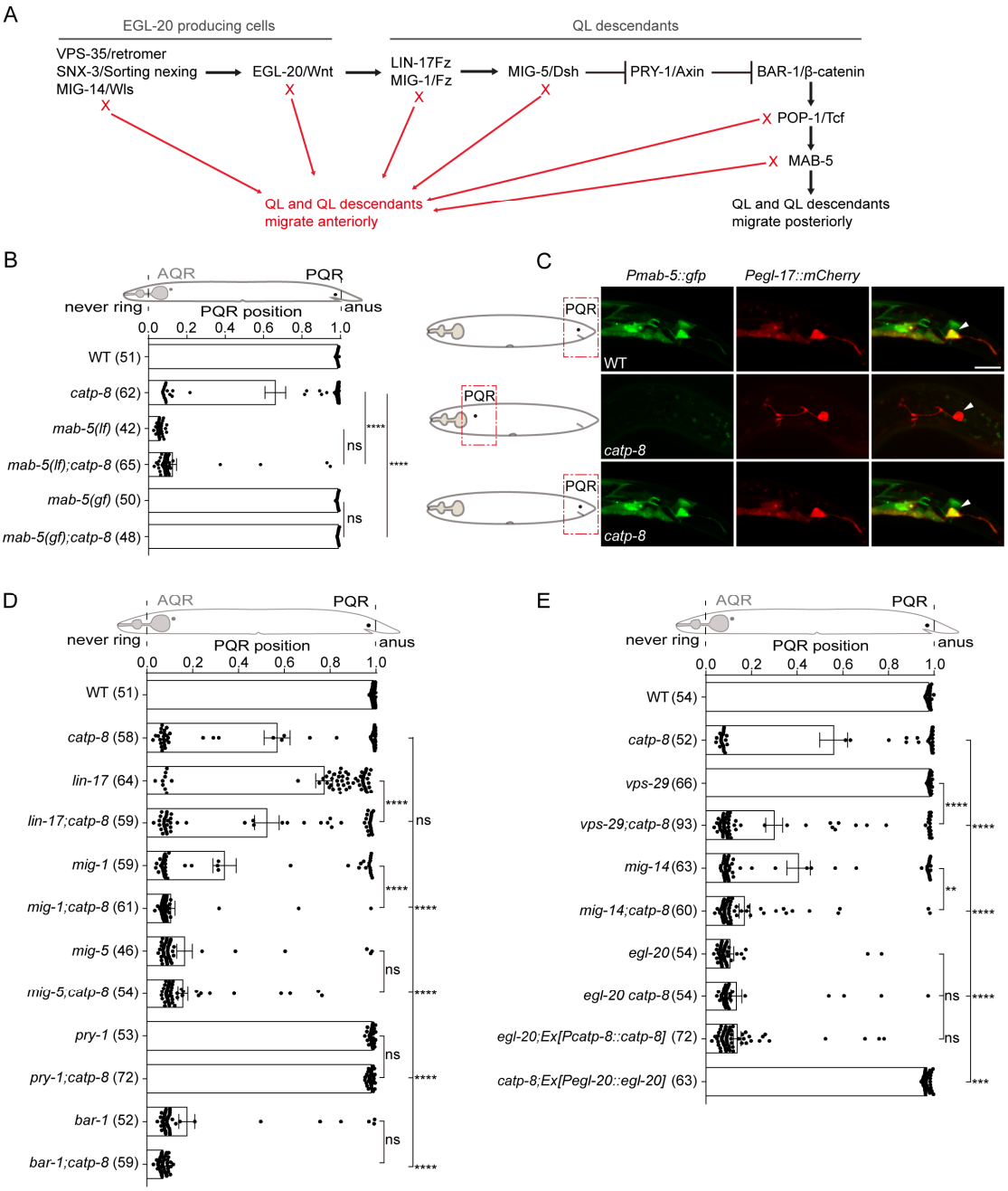

Figure 2

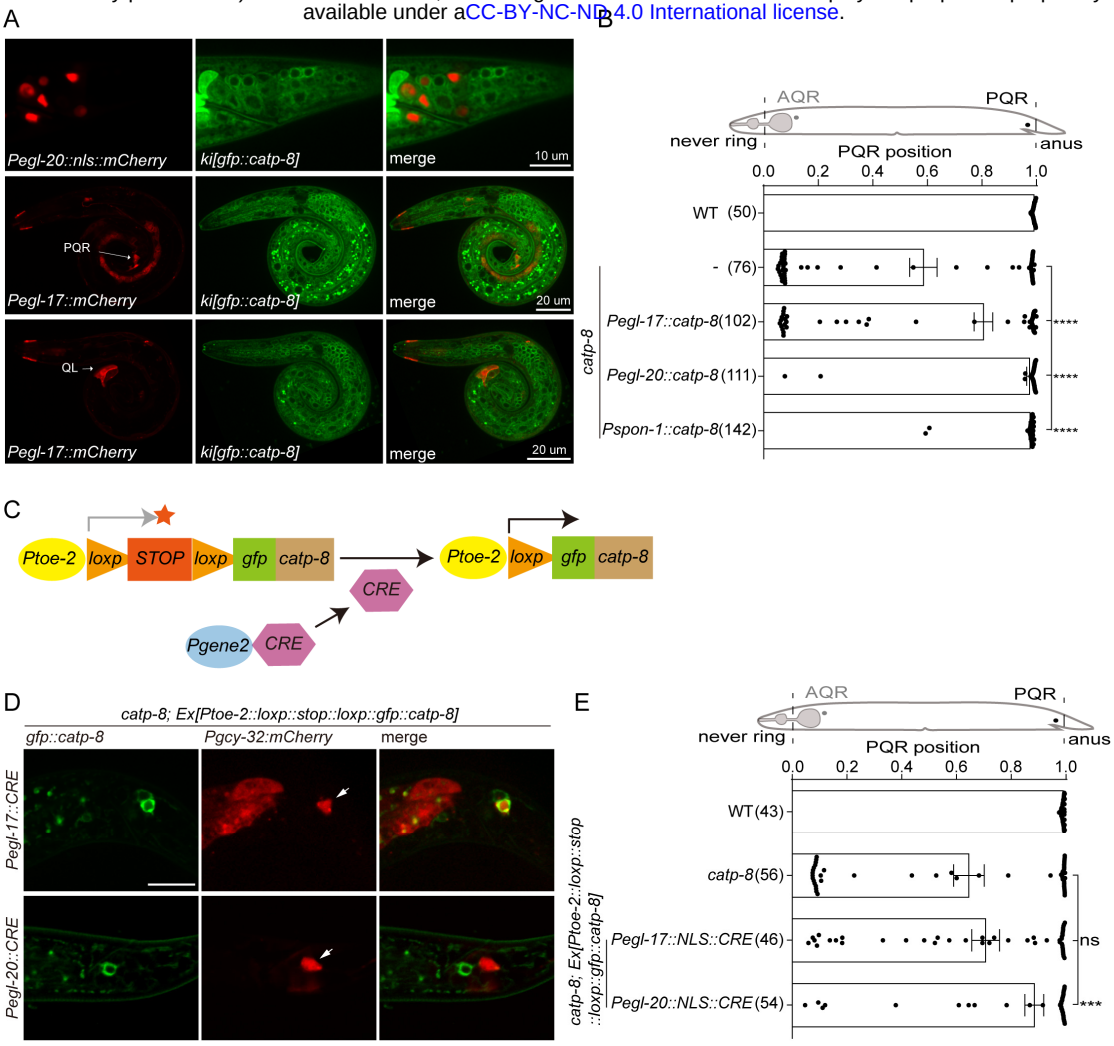

Figure 3

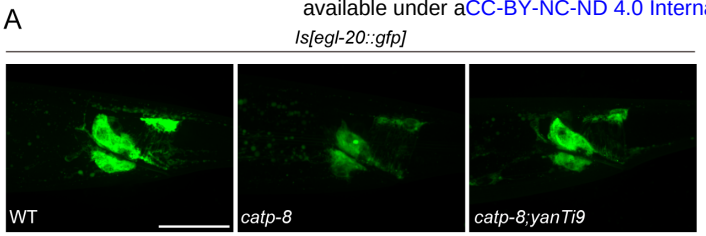

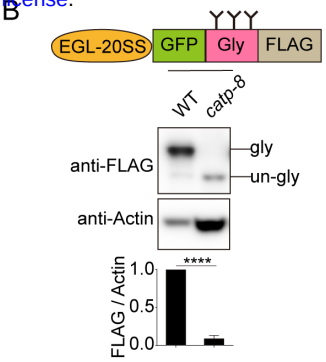

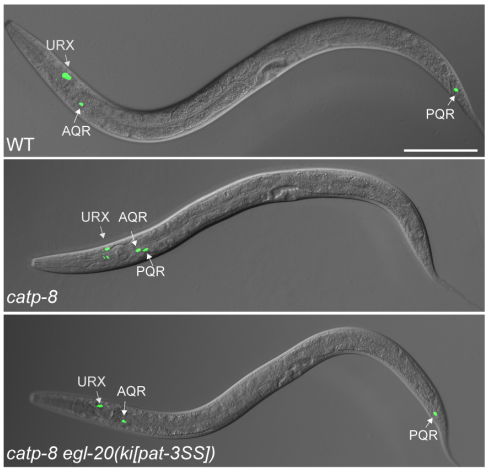

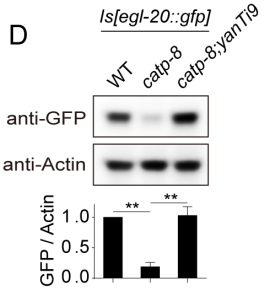

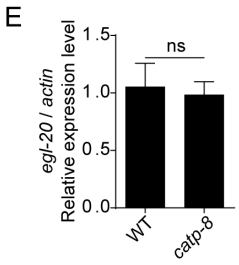

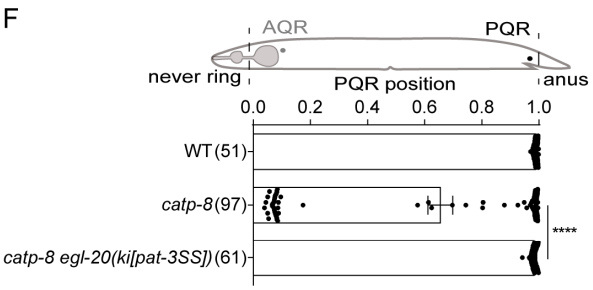

G

Name	N-terminal signal sequence	G predictor
EGL-20SS	MQFFICLIFLFVLLVYGQ	-1.776
EGL-20SS(M)	MQFFILLLIFLFVLLVYGQ	-2.802
PAT-3SS	MPPSTSLLLLAALLPFALP	1.371
PAT-3SS(M)	MPPSTSLLLLLLLLFLLLPFALPA	-2.770

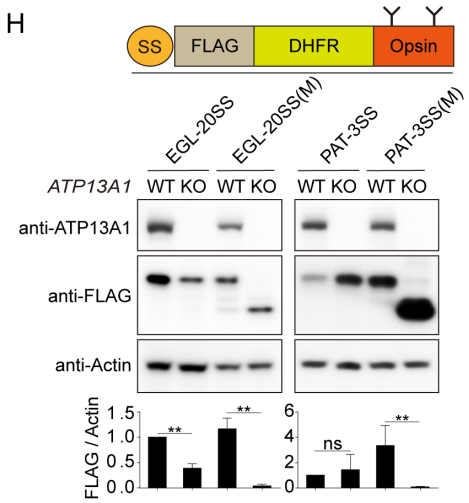

Figure 4

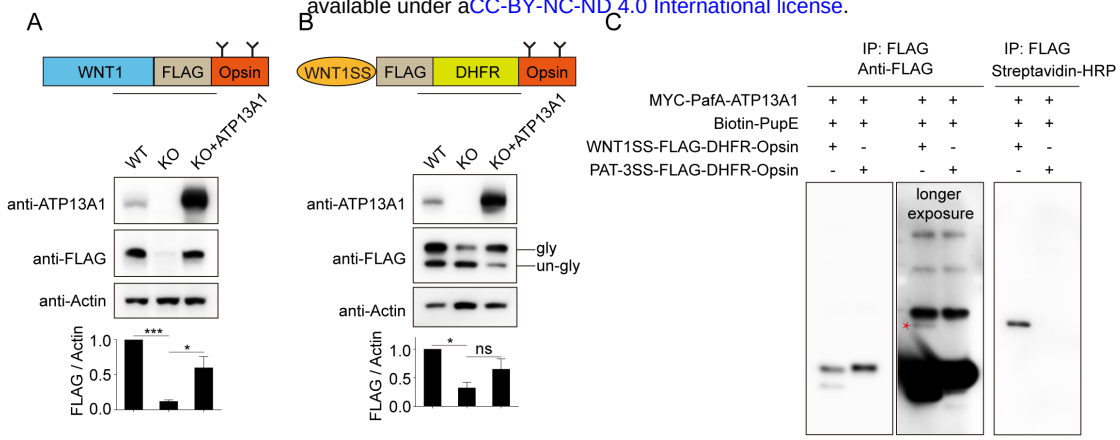

Figure 5

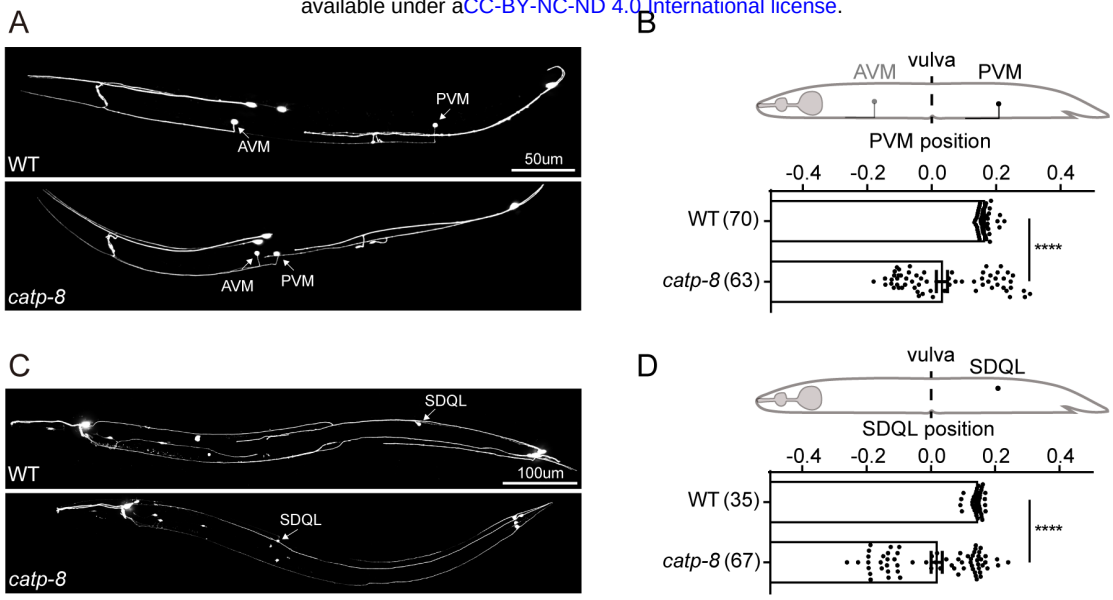

Figure S1